Improved Model of Radial Vibration in Switched Reluctance Motor Including Magnetic Saturation

Xiaoqiang Guo, *Student Member, IEEE*, Rui Zhong, Mingshu Zhang, Desheng Ding, and Weifeng Sun, *Senior Member, IEEE*

***Abstract*—This paper proposes an improved method for the prediction of radial vibration in switched reluctance motor (SRM) considering magnetic saturation. In this paper, the basic modeling principle is briefly introduced, it is based on the derivation that the peak acceleration is dependent on the product of phase current and current gradient *idi/dt*. However, the derivation may cause errors due to saturation effect. Thus in this paper, the discrete sample data are firstly acquired based on DC pulse measurement method, by which electromagnetic, torque and peak acceleration characteristics can all be acquired. Then the entire peak acceleration characteristics are obtained by improved Least Square Support Vector Machine (LSSVM). Based on the obtained static peak acceleration characteristics, the time-varied radial vibration model is established based on superposition of natural oscillations of dominant vibration modes. Finally, a simulation model is built up using MATLAB/Simulink. The good agreement between simulation and experiment shows that the proposed method for modeling is feasible and accurate, even under saturation. In addition, since LSSVM does not need any prior knowledge, it is much easier for modeling compared with other existing literatures.**

***Index Terms*—Acoustic noise, magnetic saturation, least square support vector machine, LSSVM, MIMO, modeling, radial vibration, switched reluctance motor.**

I. Introduction

ACOUSTIC noise is one of the main drawbacks in switched reluctance motor (SRM). It is widely recognized that the acoustic noise mainly originates from torque ripple and radial vibration. For the reduction of torque ripple, smooth torque control is greatly researched [1-2]. However, it is widely accepted by many researchers that radial vibration is more significant to acoustic noise than torque ripple [3-29]. Thus investigation into radial vibration is of great significance.

Many researchers have done a lot of work on the reduction of radial vibration and acoustic noise. They are mainly divided into two categories: motor design and control method. For motor design aspect, [5-9] investigated the influence of different motor structures on the mode shapes and resonant frequencies, such as yoke thickness of stator, stator pole arc, shape of frame, ribs, stack length and mounting effects. [10] compared the vibration and noise between 12/8 and 6/4 structures. [11, 12] investigated that the vibration and noise can be reduced by skewing the stator and rotor poles. In [13], a double-stator SRM is developed, which can reduce radial force, and thus to reduce vibration and noise. [14] proposed a cylindrical rotor design, which can reduce wind loss and acoustic noise simultaneously. [15] compared the radial magnetic force of the half and full-teeth-wound windings.

As is well-known that, the motor design and manufacture process will usually cost more time than control method, and even more cost. Thus control optimization is recently attracting much more concern by researchers. A typical method is two-step or namely active vibration cancellation (AVC) method [16, 17]. [18] proposed current shaping method in order to eliminate the third harmonic component of radial force. [19] analyzed the effect of randomizing turn-on angle method control parameters on the reduction of resonance noise. In [20] an advanced method of two-phase excitation based on C-dump converter is proposed, which reduces abrupt change of radial fore when phase current is extinguished. Other advanced control methods such as sinusoidal current control based on a mutually couples SRM [21] is also proposed recent years.

Although the effects of motor structures and control parameters on radial vibration have been greatly investigated, the origin and dynamic model of radial vibration still have not been fully studied, especially under magnetic saturation condition. In [22], the acceleration is computed by modal superposition. However, the method above is based on the value of radial force. Methods for radial force calculation were investigated either by analytical method [23] or finite element analysis (FEA) method [24]. However, the value of calculated radial force cannot be verified since it is hard to be measured. In addition, the accurate transfer function between radial force and vibration is hard to be obtained. Since the vibration is an electric-magnetic-force -vibration coupled problem, the radial vibration will be calculated by several steps, error caused each

Manuscript was submitted for review on 15, June, 2018.

This work was supported by the National Natural Science Foundation of China under Grant 51277026 and 61674033, Natural Science Foundation of Jiangsu Province under Grant BK20161148, and the Scientific Research Foundation of Graduate School of Southeast University under Grant YBJJ1822. (Corresponding author: Weifeng Sun.)

The authors would like to thank Xi'an Jiuchi Electromechanical Science and Technology Ltd. for its finance support and Nanjing Integrated Circuit Industry Service Center for its equipment support and logistics service.

The authors are with the National ASIC System Engineering Research Center, Southeast University, Nanjing 210018, China (e-mail: wuxigxq@seu.edu.cn; ray@seu.edu.cn; 2471815151@qq.com; dds@seu.edu.cn; swffrog@seu.edu.cn). Weifeng Sun is also with Power Devices and Integration Engineering Department, Collaborative Innovation Center of IC Design and Manufacturing of Yangtze River Delta, Shanghai, 201203, China.

Digital Object Identifier 10.30941/CESTEMS.2018.00046

step will be accumulated and enlarged, which will finally cause great errors in the estimation of radial vibration.

So recently, investigated into the relation between radial vibration and electrical parameters has raised more concern. Thus the problem can be simplified as electric-vibration problem. It was found that the maximum radial vibration, i.e. peak acceleration shown in Fig. 1, occurs at turn-off instant. Then the vibration will oscillate at the resonant frequencies naturally, which is called natural oscillation. In [25], the origin of peak acceleration was investigated and found that the peak acceleration is caused by the abrupt change of phase voltage, which changes from $+U$ to $-U$. After peak acceleration, the motor produces damped oscillations consisting of several natural vibration modes. However, the relation between the abrupt change of phase voltage and peak acceleration was not described, and only one natural vibration mode was included in the model. In [26], the origin of peak acceleration is analytically derived, which revealed that the abrupt change of phase voltage will cause sudden change of power, i.e. energy, and thus initiate radial vibration. However, the derivation of fourth order state space method is rather complicated. In [27], the authors have analytically derived that the value of peak acceleration is dependent on the product of phase current and current gradient. However, the saturation is not considered.

This paper is mainly improved work based on [27]. The principle of modeling, i.e. work in [27] is firstly briefly introduced. Then due to neglect of magnetic saturation in [27], the paper will fully investigate the peak acceleration by DC pulse measurement method, and some sample data of both electromagnetic and peak acceleration are acquired. Due to the advantage of no prior knowledge, an improved least square support vector machine (LSSVM) is used to obtain the entire peak acceleration characteristics. Based on the obtained static peak acceleration characteristics, the time-varied radial vibration is analytically modeled based on the superposition of natural oscillations of each vibration mode. Finally, simulation model is built up based on MATLAB/Simulink and an experimental setup is also established to verify the proposed improved model.

The main contribution of this paper is as follows: 1) Investigation of peak acceleration for both linear and saturation conditions by DC pulse measurement method. 2) The entire peak acceleration model is established using an improved LSSVM, which does not need any prior knowledge.

This paper is organized as follows: Section II briefly introduces the principle of modeling. Section III gives the process of data acquisition in detail. The simulation model is built up in Section IV. And Section V establishes the experimental setup and verifies the proposed improved method by comparing the simulation and experiment results. And section VI gives the conclusion and discussion.

II. Basic Principle of Radial Vibration Modeling

A. Basic principle

The authors have previously derived the relationship between peak acceleration and product of phase current and

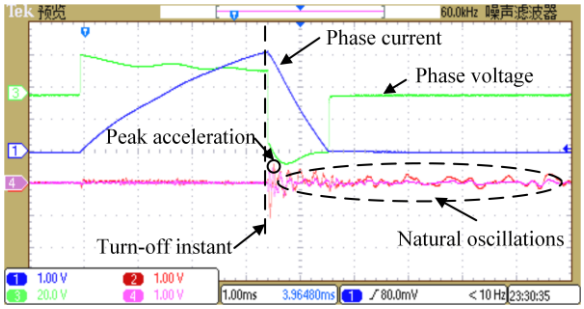

Fig. 1. Radial vibration composition: peak acceleration at turn-off instant and natural oscillations afterwards.

current gradient in [27]. It is well-known that the vibration is highly relevant to the radial force gradient, thus it is recognized that the vibration is mainly caused by the rapid change of radial force at turn-off instant.

The inductance L can be expressed as (1) [5] when saturation is not considered,

$$L = \frac{\mu_0 N^2 l R}{g} f(\theta_{ovl}) \tag{1}$$

where μ_0 is the permeability of air, N is turns of winding for each stator pole, l is the stack length, R is the outer radius of rotor, g is the length of air gap, and $f(\theta_{ovl})$ is a linear function of overlapping angle between stator and rotor poles as (2).

$$f(\theta_{ovl}) = p\theta_{ovl} + q \tag{2}$$

and

$$\theta_{ovl} = \begin{cases} 0, & \theta \le 6.5° \\ \dfrac{\pi}{180°}(\theta - 6.5°), & 6.5° < \theta \le 21.5° \\ \dfrac{\pi}{12}, & 21.5° < \theta \le 22.5° \end{cases} \tag{3}$$

where p and q are linear function coefficients, 0º is the unaligned position and 22.5º is the aligned position in the sample motor, the detailed specifications of which is listed in Table I. Since the stator and rotor arcs are 15º and 17º respectively, 6.5º is the position where rotor and stator poles start to overlap.

Accordingly, the radial force F_r can be calculated as (4) based on the virtual displacement method [23].

$$F_r = \frac{\partial W_{co}}{\partial g} = \frac{\partial\left(\frac{1}{2}Li^2\right)}{\partial g} = \frac{1}{2}K_f i^2 f(\theta_{ovl}) \tag{4}$$

where W_{co} is co-energy, $K_f = -\mu_0 N^2 l R / g^2$, which is a constant.

Further the radial force gradient can be obtained as (5).

$$\begin{aligned} \frac{dF_r}{dt} &= \frac{\partial F_r}{\partial \theta}\frac{d\theta}{dt} + \frac{\partial F_r}{\partial i}\frac{di}{dt} \\ &= \frac{1}{2}K_f i^2 \omega f'(\theta_{ovl}) + K_f i \frac{di}{dt} f(\theta_{ovl}) \end{aligned} \tag{5}$$

For simplicity, suppose that there's a linear relationship between peak acceleration and radial force gradient at turn-off instant, peak acceleration can be expressed as (6).

$$a_p = K_a \frac{dF_r}{dt} = \frac{1}{2}K_g i^2 \omega f'(\theta_{ovl}) + K_g i \frac{di}{dt} f(\theta_{ovl}) \tag{6}$$

where a_p is peak acceleration, K_a is the coefficient, and K_g =

$K_a \cdot K_f$, which is also a constant.

It can be seen from (6) that, when the rotor is locked, the speed is zero, thus the first item is ignored, (6) can be simplified as (7). And $f(\theta_{ovl})$ is also a constant at a fixed rotor position. When a DC pulse is injected into phase winding, the peak acceleration is highly dependent on the product of phase current and current gradient (idi/dt) at turn-off instant.

$$a_p = K_g i \frac{di}{dt} f(\theta_{ovl}) \tag{7}$$

Thus the static peak acceleration characteristics can be acquired by DC pulse measurement method at different idi/dt and rotor positions. Different idi/dt can be achieved by different duration of DC pulse, and different rotor positions can be implemented by rotating and fixing the rotor by rotor clamping devices. Based on the static characteristics, the value of K_g and $f(\theta_{ovl})$ can all be calculated.

For dynamic peak acceleration characteristics, formula (4) is used to calculate the peak acceleration. Since the value of K_g, $f(\theta_{ovl})$ and $f'(\theta_{ovl})$ are all known from static characteristics, formula (4) can be easily calculated based on the value of i, di/dt and ω at turn-off instant.

B. Simple demonstration of the basic principle

The principle is firstly demonstrated at three rotor positions, which are 7.5º, 15º, 22.5º. Note that, the three rotor positions are not special, and they can be randomly selected. At each rotor position, the phase winding is excited for three times. For each time, the duration of the excitation is different in order to obtain different values of idi/dt. In this way, for each rotor position, one point can be determined in a Cartesian coordinate, the value of idi/dt is x-coordinate, and peak acceleration is y-coordinate. For each rotor position, two points can determine a line, and a third point can be used to verify the line. The measured points for the three rotor positions and the curved lines are shown in Fig. 2. It can be seen from the figure that for each rotor position, the relation between peak acceleration and idi/dt is almost linear, which demonstrates the correctness of the basic principle.

III. Peak Acceleration Characteristics Obtained by DC Pulse Measurement Method and Improved LSSVM

A. DC Pulse Measurement Method and Platform

The schematic diagram and the practical platform of DC pulse measurement methods are shown in Fig. 3. The platform mainly consists of the following components:

a) Controller, which is implemented on a STM32F103 MCU.

b) A typical asymmetric half bridge power converter.

c) A 12/8 sample SRM, whose detailed specifications are listed in Table 1, with an accelerometer attached on the surface of the frame of the sample motor, whose output sensitivity is 250mV/g within 0.5Hz ~ 12kHz.

d) A mechanical rotor clamping device used to fix the rotor of the sample motor, whose sensitivity is 0.5º/div.

e) Current hall sensors, whose sensitivity are 4V /300A.

f) Tektronix DPO2024 oscilloscope with probes, which can measure phase voltage directly.

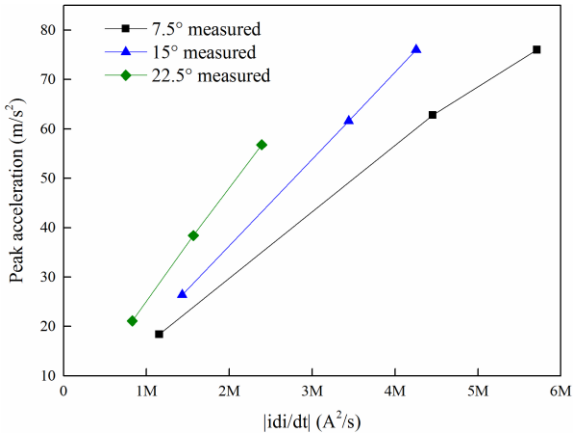

Fig. 2. Sampled peak acceleration vs. idi/dt at three rotor positions.

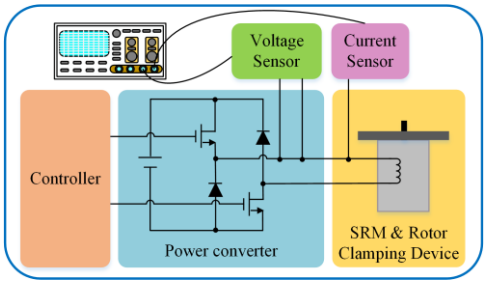

(a) Schematic diagram

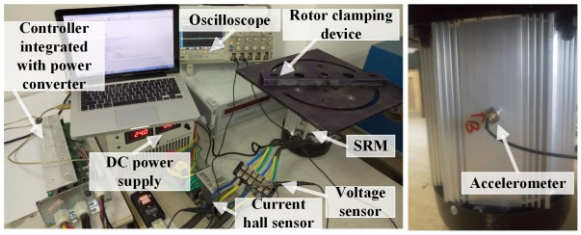

(b) Practical platform

Fig. 3. Introduction of DC pulse measurement method.

TABLE I
MOTOR SPECIFICATIONS

Parameter	Value
Number of phases	3
Number of stator and rotor poles	12/8
Stator outer diameter	160mm
Thickness of stator yoke	12.5mm
Rotor outer diameter	94.2mm
Shaft diameter	29mm
Air gap length	0.4mm
Stator pole arc	15º
Rotor pole arc	17º
Stack length of stator/rotor	140mm
Rated voltage	72V
Rated power	4kW
Rated speed	2800rpm
Rated torque	13.6Nm

The rotor is firstly mechanically fixed at the aligned position, which is much easier to be found either by DC current supply or maximum inductance measurement. Then a DC pulse with a particular duration is injected into a phase winding, the phase voltage and corresponding current and vibration response, and the calculated current gradient are all shown in Fig. 4. By this way, one group of phase current, current gradient, rotor

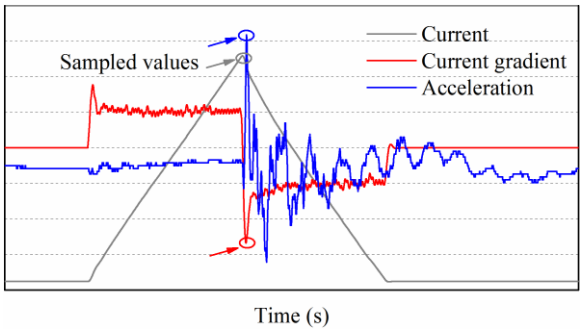

Fig. 4. Sampled current, current gradient and peak acceleration at a fixed rotor position.

position and peak acceleration is recorded, circled in Fig. 4. By tuning the time duration of DC pulse and rotor position, different groups of sample data can be recorded, including the magnetic saturation effect, as long as the time duration is long enough for phase current to enter saturation condition.

On the other hand, sample data of electromagnetic characteristics can also be indirectly measured. Since the phase voltage and current are sampled, the flux linkage can be calculated by the improved Euler's formula [28]. Consequently, the torque characteristics can be calculated which is also based on the virtual displacement method.

Thus it can be seen from the introduction above that, not only peak acceleration characteristics, but also electromagnetic and torque characteristics can all be obtained through DC pulse measurement method, which takes less steps in the entire vibration modeling process, and is much easier than the multi-physics modeling method [29].

B. Entire Static Characteristic Obtained by Improved LSSVM

The discrete sample data are obtained by DC pulse measurement method. The traditional methods for obtaining the entire characteristics are mainly look-up table or curving functions. However, the accuracy of the model based on such methods will highly depend on the amount of sample data. This disadvantage can be overcome by some artificial intelligent methods, such as fuzzy logic algorithm, neural network and so on. Among them, neural network is the mainstream. However, they all need prior knowledge and depend on the experience of developers. Thus in this paper, LSSVM [39] is used to overcome the two disadvantages above. In addition, LSSVM can solve the problems of over-fitting, early plunge into local minimum, curse of dimensionality, and so on, which are superior advantages compared with neural network. Since LSSVM is a method based on statistical learning theory, which is in specialty applied on machine learning theory with limited amount of samples, thus LSSVM is the best theory for statistical estimation and learning with limited samples.

The training and testing processes of electromagnetic and torque characteristics have been introduced in [28]. The following section will introduce the training and testing process of peak acceleration process in detail.

The schematic diagram of static peak acceleration model is shown in Fig. 5. In this paper, 168 groups of data are sampled at 24 rotor positions (0º ~ 22.5º with interval of 0.5º or 1.0º) and 7

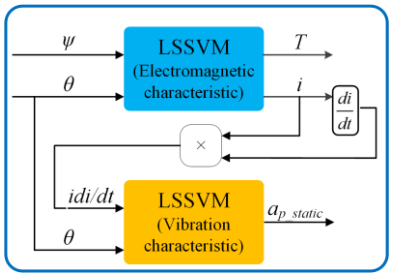

Fig. 5. Structure of static peak acceleration model.

currents (0A ~ 240A, interval is different for each rotor position, since peak current at turn-off instant cannot be accurately controlled). Then all currents are used and only a quarter of the rotor positions are used as training set to train LSSVM. The left are used as test set to verify the performance of the LSSVM. Thus 63 groups of data are used as training set, and 105 groups of data are used as test set.

The predicted peak acceleration using LSSVM and measured values of both training set and test set are shown in Fig. 6. And the absolute errors, which are defined by equation (8), of both sets are shown in Fig. 7. It can be seen that the accuracy of training set are rather high, while the error of test set is a little larger than that of training set. However, since the maximum absolute error of test set is only 2.45m/s^2, the accuracy can be fully accepted.

LSSVM has the advantage of no prior knowledge compared with other artificial intelligent method. In addition, although it need more calculation steps and time compared with the simplest method interpolation, the accuracy can be greatly improved. The relative error waveforms of the test data by both LSSVM and 2D interpolation method are shown in Fig. 8. And the detailed performance by these two methods are compared in Table II, where ε_{mae}, ε_{mare} and ε_{rmse} are the maximum absolute error, maximum absolute relative error, and root mean square error, which are defined in equation (8)-(10), respectively. And c, σ, d are the regularization parameter, RBF kernel width coefficient and polynomial kernel order.

$$\varepsilon_{mae} = \max\left(\left|y_p - y_m\right|\right) \tag{8}$$

$$\varepsilon_{mare} = \max\left(\left|\frac{y_p - y_m}{y_m}\right|\right) \tag{9}$$

$$\varepsilon_{rmse} = \sqrt{\frac{\sum_{i=1}^{N}\left(y_p - y_m\right)^2}{N}} \tag{10}$$

It can be seen in Fig. 8 and Table II that compared with 2D interpolation, the accuracy the model can be improved by more than 35% using LSSVM. Although the training and calculation time of LSSVM is 6.281ms, which is nearly two times larger than 3.205ms of 2D interpolation, whereas the time level of ms is fully acceptable in modern computer.

C. Entire Static Characteristic Obtained by Improved LSSVM

The static peak acceleration characteristics have been obtained by direct measurement and LSSVM. However, when the motor is operated under rotational condition, the peak

acceleration may have even larger errors. This is due to neglect of first item in equation (6). Thus the dynamic peak acceleration can be obtained by the composition of first item calculation and LSSVM, shown in Fig. 9.

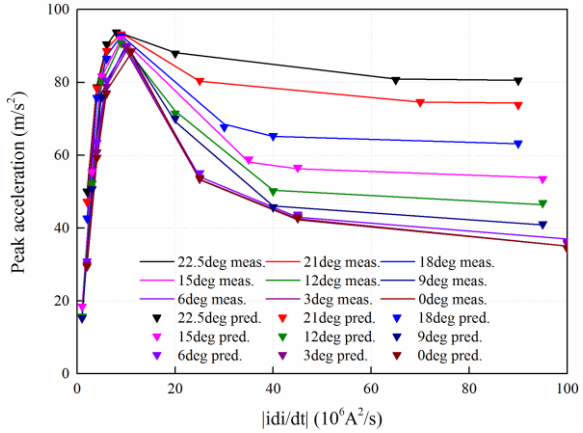

(a) Training set

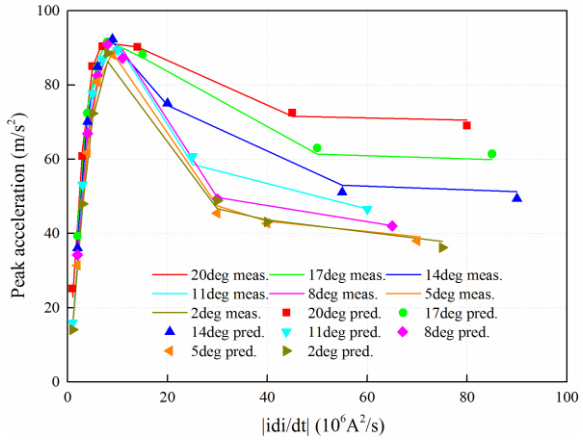

(b) Test set

Fig. 6. Predicted and measured peak acceleration of training set and test set

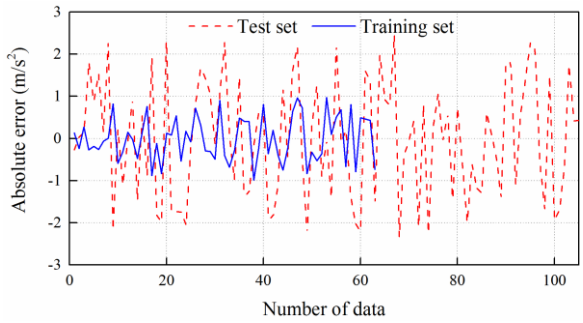

Fig. 7. Comparison of absolute error between training set and test set

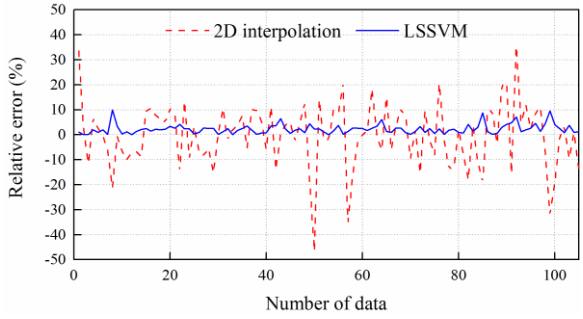

Fig. 8. Comparison of relative error of test set by LSSVM and 2D interpolation

TABLE II
COMPARISON OF RESULTS BETWEEN LSSVM AND 2D INTERPOLATION

Model type		LSSVM	2D interpolation
ε_{mae} (m/s^2)		2.45	9.97
ε_{mare} (%)		9.98	46.53
ε_{rmse} (m/s^2)		1.37	5.71
Optimal parameters	c	20	-
	σ	0.05	-
	d	5	-
Training and calculation time (ms)		6.281	3.205

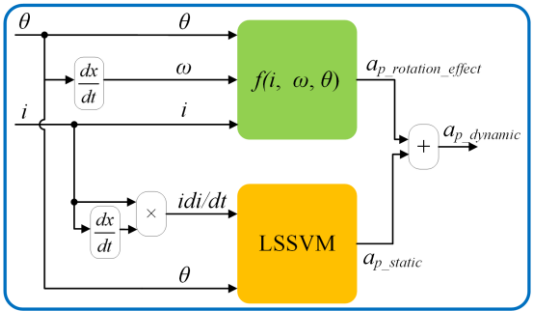

Fig. 9. Schematic diagram of dynamic peak acceleration model.

When peak acceleration is obtained, the acceleration of each vibration mode can be calculated by weight factors. In addition, other critical parameters such as natural frequencies and damping ratio can also be obtained by various methods [5-9, 26, 27, 29]. Thus as long as the parameters above are known, the overall radial vibration can be solved as (11) [27].

$$a(t)=\sum_i a_{pi}e^{-\zeta_i\omega_{ni}t}\left[\cos\left(\sqrt{1-\zeta_i^2}\,\omega_{ni}t\right)-\frac{\zeta_i}{\sqrt{1-\zeta_i^2}}\sin\left(\sqrt{1-\zeta_i^2}\,\omega_{ni}t\right)\right] \quad (11)$$

IV. SIMULATION MODEL

The simulation model is built up based on MATLAB/Simulink, which is shown in Fig. 10. Fig. 10(a) shows the simulation model of single phase, including converter module, angular transformation module, electromagnetic model, dynamic peak acceleration model and natural oscillation model. And the detailed model of dynamic peak acceleration is shown in Fig. 10(b). It can be seen that the static peak acceleration is predicted by LSSVM. Then the value of static peak acceleration is compensated with the rotational effect when is motor is under rotating condition. However, as peak acceleration occurs only at turn-off instant. The predicted value will be output only at turn-off instant, which can be implemented by a triggered system that detects the 'OR' logic of two switch signals. In addition, at the turn-off instant, the time will be reset to zero, thus the natural oscillation can be initiated from zero at each turn-off instant.

V. EXPERIMENTAL VERIFICATION

A. Experimental Setup

The experimental setup is mainly consists of the sample motor, controller, DC power supply, oscilloscope, magnetic powder brake and dynamometer, which are shown in Fig. 11. For easy identification, the acceleration attached on sample motor is shown in its enlarged form.

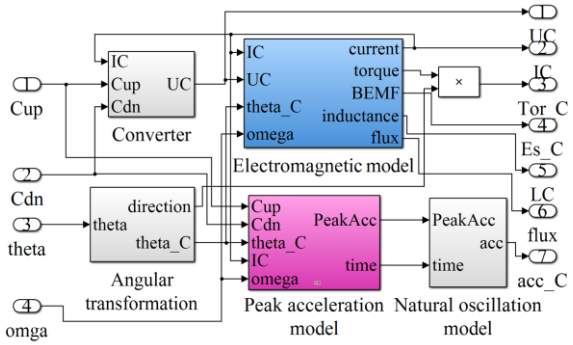

(a) Single phase model

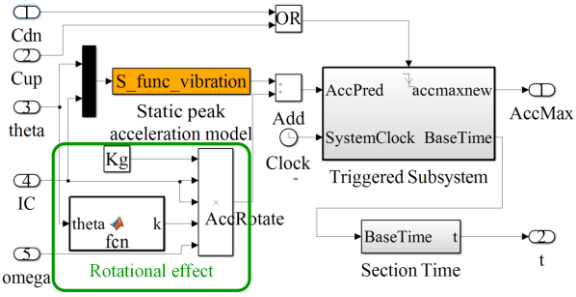

(b) Dynamic peak acceleration model

Fig. 10. Simulation model based on MATLAB/Simulink.

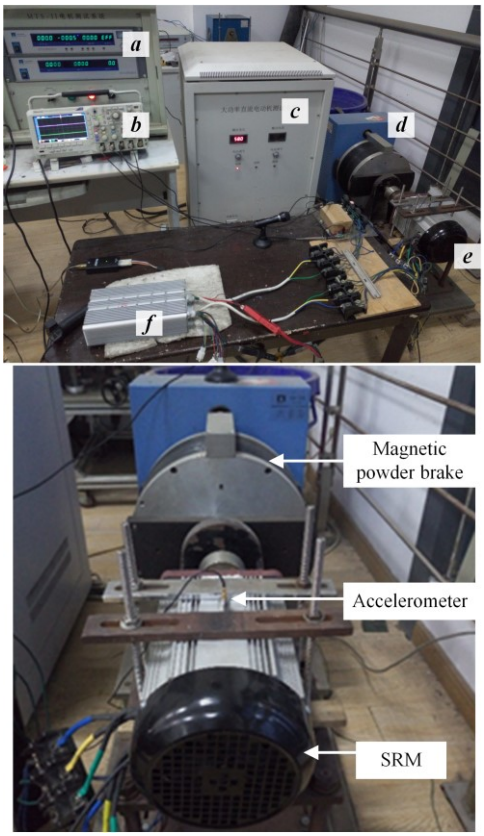

Fig. 11 Photograph of dynamic experimental setup (a) Dynamometer (b) Oscilloscope (c) DC power supply (d) Magnetic powder brake (e) 12/8 sample motor (f) Controller

B. Comparison Between Simulation and Experimental Results

The simulation and experiment are both conducted to verify the effectiveness and accuracy of the proposed method. The simulation and experiment are conducted under angle position control (APC) mode, which is typical control mode in SRM. And the turn-on and turn-off angles can be randomly selected to verify the effectiveness. In this paper, -6º and 12º are selected, which are optimal switch angles by trial and error in real working condition. In addition, pulse width modulation (PWM) is used for speed regulation. The sampling rate of current and acceleration in experiments are both100MHz.

Unsaturated condition: Firstly, light load is selected to verify the accuracy of the proposed model under un-saturated condition. The load torque is selected as 13.5Nm, which is rated load of the sample motor. And the duty ratio in this condition is 75% in order to avoid saturation as possible. The time domain of simulated and experimental vibration waveforms are shown in Fig. 12(a). It can be seen that the overall shapes of radial vibration between simulation and experiment are almost the same, which demonstrates that the proposed method is feasible. Then the maximum absolute relative error of peak acceleration is about 14.8%, when the experimental and simulation values are 61m/s^2 and 52m/s^2, respectively, which can be acceptable in practical engineering. In addition, it is known that the acoustic noise is much sensitive to frequency. Thus comparing the spectrums of simulation and experiment waveforms in Fig. 12(b), it can be found that the dominant frequencies and corresponding amplitude are rather consistent (17.8m/s^2 and 18.5m/s^2 at about850Hz, and 8.3m/s^2 and 8.1m/s^2 at about 6425Hz), which can further demonstrate the feasibility and accuracy of the proposed model.

Saturated condition: Then the proposed model is verified under saturated condition. The load torque is selected as 33Nm which is more than two times larger than the rate load, thus the motor will easily be operated into magnetic saturation condition. In addition, duty ratio of PWM is 100% in order to make the inductance saturated as possible.

The time domain of simulated and experimental vibration waveforms are shown in Fig. 13(a). It can be seen that the vibration waveforms are also almost the same between simulation and experiment results, especially the low frequency oscillation. However, the vibration of high frequencies is not fully consistent between simulation and experiment, resulting in relatively large errors in peak acceleration which is more than 30%. This can be influenced by many other mechanical factors, such as vibration by end cover, bearing, mounting, magnetic power brake and so on, which are not main focuses in this paper. However, the accuracy of the proposed method under saturated condition can still be verified by spectrum of vibration. It can be seen from Fig. 13(b) that the amplitudes of the most dominant frequency at 850Hz by simulation and experiment are 16m/s^2 and 16.5m/s^2, respectively, whose relative error is only 3%. The estimated errors in high frequencies, similar as time frequency, can also be seen in spectrum domain. However, as the highest speed in the sample motor is about 8400rpm, the highest excitation frequency of three phases is 3360Hz, which is much lower than the 4th order natural frequency 6.4kHz. Thus although the predicted amplitudes in high frequencies may have some errors, this will not cause influence the analysis of acoustic noise, since it shows that the low frequency vibration is much more important to acoustic noise.

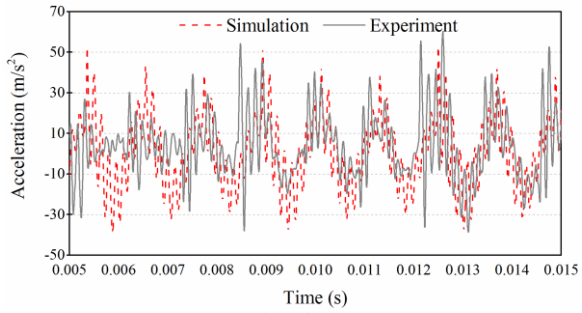

(a) Time domain

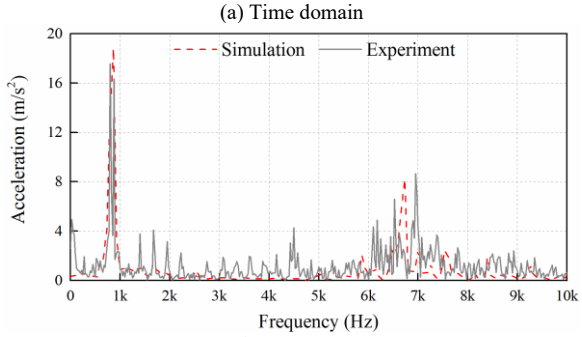

(b) Spectrum

Fig. 12 Radial vibration and spectrum comparison under un-saturated condition between simulation and experiment (Load: 13.5Nm, speed: 2100rpm, PWM 75%)

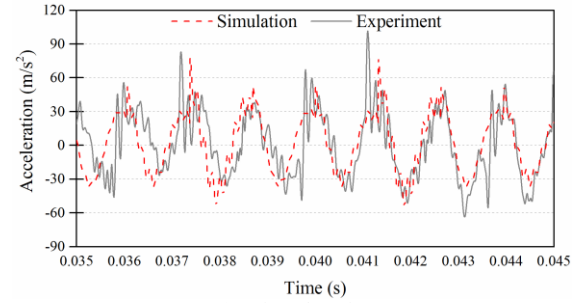

(a) Time domain

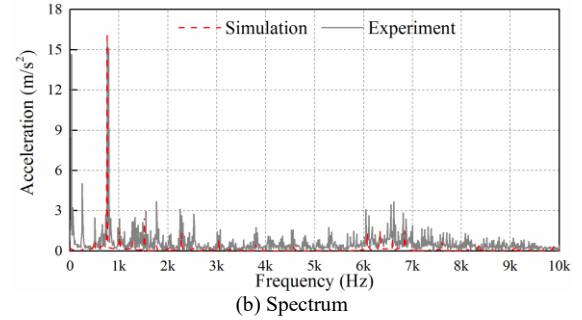

(b) Spectrum

Fig. 13 Radial vibration and spectrum comparison between simulation and experiment (Load: 33Nm, speed: 1900rpm, PWM 100%).

VI. Conclusion and Discussion

This paper proposes an improved model of [27] of radial vibration including magnetic saturation based on direct measurement and improved LSSVM. It is based on the derivation that the peak acceleration is dependent on the value of *idi/dt* at turn-off instant. Compared with the traditional multi-physics method, i.e. radial force calculation based method, such as [29], the accuracy is greatly improved. In [29], although the radial force is calculated by FEA, it has not been verified by measurement. Only the resultant radial vibration is compared between simulation and experiment. The acceleration at second order vibration mode frequency of simulation and experiment results are approximately 6.4m/s^2 and 1.2m/s^2, whose relative error exceeds 433%. Compared with previous work in [27], which only considers linear induction region, the accuracy of improved model can be greatly improved in inductance saturated region. In [27], the simulated and experimental amplitudes of dominant vibration mode are 18.8m/s^2 and 17.6m/s^2, whose relative error is 6.8%. While in the proposed method in this paper, when under even more heavy load than [27] (28Nm in [27], and 33Nm in this paper), the acceleration of simulation and experiment results at the dominant vibration mode frequency are 16m/s^2 and 16.5m/s^2, whose relative error is only 3%.

References

[1] Ralev, I., Qi, F., Burkhart, B., Klein-Hessling, A., and De Doncker, R.W., 'Impact of Smooth Torque Control on the Efficiency of a High-Speed Automotive Switched Reluctance Drive', *IEEE Transactions on Industry Applications*, 2017, pp. 1-1.

[2] Ye, J., Bilgin, B., and Emadi, A., "An Offline Torque Sharing Function for Torque Ripple Reduction in Switched Reluctance Motor Drives", *IEEE Transactions on Energy Conversion*, vol. 30, no. 2, pp. 726-735, 2015.

[3] H. J. Wang, J. F. Bao, B. K. Xue, J. F. Liu, "Control of Suspending Force in Novel Permanent-Magnet-Biased Bearingless Switched Reluctance Motor," *IEEE Transactions on Industrial Electronics*, vol. 62, pp. 4298-4306, 2015.

[4] M. Boesing, A. Hofmann, and R. De Doncker, "Universal acoustic modelling framework for electrical drives," *IET Power Electronics*, vol. 8, pp. 693-699, 2015.

[5] Colby, R.S., Mottier, F.M., and Miller, T.J.E., 'Vibration Modes and Acoustic Noise in a Four-Phase Switched Reluctance Motor', *IEEE Transactions on Industry Applications*, vol. 32, no. 6, pp. 1357-1364, 1996.

[6] Besbes, M., Picod, C., Camus, F., and Gabsi, M., 'Influence of Stator Geometry Upon Vibratory Behaviour and Electromagnetic Performances of Switched Reluctance Motors', *IEE Proceedings-Electric Power Applications*, vol. 145, no. 5, pp. 462-46, 1998.

[7] Cai, W. and Pillay, P., 'Resonant Frequencies and Mode Shapes of Switched Reluctance Motors', *IEEE Transactions on Energy Conversion*, vol. 16, no. 1, pp. 43-48, 2001.

[8] Jianbo, S., Qionghua, Z., Shuanghong, W., and Zhiyuan, M., 'A Novel Radiating Rib Structure in Switched Reluctance Motors for Low Acoustic Noise', *IEEE Transactions on Magnetics*, vol. 43, no. 9, pp. 3630-3637, 2007.

[9] Castano, S.M., Bilgin, B., Fairall, E., and Emadi, A., 'Acoustic Noise Analysis of a High-Speed High-Power Switched Reluctance Machine: Frame Effects', *IEEE Transactions on Energy Conversion*, vol. 31, no. 1, pp. 69-77, 2016.

[10] Li, J., Song, X., and Cho, Y., 'Comparison of 12/8 and 6/4 Switched Reluctance Motor: Noise and Vibration Aspects', *IEEE Transactions on Magnetics*, vol. 44, no. 11, pp. 4131-4134, 2008.

[11] Yang, H.Y., Lim, Y.C., and Kim, H.C., 'Acoustic Noise/Vibration Reduction of a Single-Phase Srm Using Skewed Stator and Rotor', *IEEE Transactions on Industrial Electronics*, vol. 60, no. 10, pp. 4292-4300, 2013.

[12] Gan, C., Wu, J.H., Shen, M.J., Yang, S.Y., Hu, Y.H., and Cao, W.P., 'Investigation of Skewing Effects on the Vibration Reduction of Three-Phase Switched Reluctance Motors', I*EEE Transactions on Magnetics*, vol. 51, no. 9, 2015.

[13] Isfahani, A.H. and Fahimi, B., 'Comparison of Mechanical Vibration between a Double-Stator Switched Reluctance Machine and a Conventional Switched Reluctance Machine', *IEEE Transactions on Magnetics*, vol. 50, no. 2, 2014.

[14] Kiyota, K., Kakishima, T., Chiba, A., and Rahman, M.A., 'Cylindrical Rotor Design for Acoustic Noise and Windage Loss Reduction in Switched Reluctance Motor for Hev Applications', *IEEE Transactions on*

Industry Applications, vol. 52, no. 1, pp. 154-162, 2016.

[15] Hua, W., Hua, H., Dai, N., Zhao, G., and Cheng, M., 'Comparative Study of Switched Reluctance Machines with Half-and Full-Teeth-Wound Windings', *IEEE Transactions on Industrial Electronics*, vol. 63, no. 3, pp. 1414-1424, 2016.

[16] Long, S.A., Zhu, Z.Q., and Howe, D., 'Effectiveness of Active Noise and Vibration Cancellation for Switched Reluctance Machines Operating under Alternative Control Strategies', *IEEE Transactions on Energy Conversion*, vol. 20, no. 4, pp. 792-801, 2005.

[17] Makino, H., Kosaka, T., and Matsui, N., 'Digital Pwm-Control-Based Active Vibration Cancellation for Switched Reluctance Motors', *IEEE Transactions on Industry Applications*, vol. 51, no. 6, pp. 4521-4530, 2015.

[18] Takiguchi, M., Sugimoto, H., Kurihara, N., and Chiba, A., 'Acoustic Noise and Vibration Reduction of Srm by Elimination of Third Harmonic Component in Sum of Radial Forces', *IEEE Transactions on Energy Conversion*, vol. 30, no. 3, pp. 883-891, 2015.

[19] Guo, X.Q.., Zhong, R., Ding, D.S.., Zhang, M.S., Shao, W.J., and Sun, W.-f., 'Origin of Resonance Noise and Analysis of Randomising Turn-on Angle Method in Switched Reluctance Motor', *IET Electric Power Applications*, vol. 11, no. 7, pp. 1324-1332, 2017.

[20] Ahn, J.W., Park, S.J., and Lee, D.H., 'Hybrid Excitation of Srm for Reduction of Vibration and Acoustic Noise', *IEEE Transactions on Industrial Electronics*, vol. 51, no. 2, pp. 374-380, 2004.

[21] Liang, X., Li, G., Ojeda, J., Gabsi, M., and Ren, Z., 'Comparative Study of Classical and Mutually Coupled Switched Reluctance Motors Using Multiphysics Finite-Element Modeling', *IEEE Transactions on Industrial Electronics*, vol. 61, no. 9, pp. 5066-5074, 2014.

[22] Torregrossa, D., Fahimi, B., Peyraut, F., and Miraoui, A., 'Fast Computation of Electromagnetic Vibrations in Electrical Machines Via Field Reconstruction Method and Knowledge of Mechanical Impulse Response', *IEEE Transactions on Industrial Electronics*, vol. 59, no. 2, pp. 839-847, 2012.

[23] Husain, O. and Anwar, M.N., 'Radial Force Calculation and Acoustic Noise Prediction in Switched Reluctance Machines', *IEEE Transactions on Industry Applications*, vol. 36, no. 6, pp. 1589-1597, 2000.

[24] Boesing, M., Hofmann, A., and De Doncker, R., 'Universal Acoustic Modelling Framework for Electrical Drives', *IET Power Electronics,* vol. 8, no. 5, pp. 693-699, 2015.

[25] Z. Q. Zhu, X. Liu, and Z. P. Pan, "Analytical Model for Predicting Maximum Reduction Levels of Vibration and Noise in Switched Reluctance Machine by Active Vibration Cancellation," *IEEE Transactions on Energy Conversion*, vol. 26, pp. 36-45, Mar 2011.

[26] C. J. Lin and B. Fahimi, "Prediction of Radial Vibration in Switched Reluctance Machines," IEEE Transactions on Energy Conversion, vol. 28, pp. 1072-1081, Dec 2013.

[27] Guo, X.Q., Zhong, R., Zhang, M.S., Ding, D.S., and Sun, W.F., 'Fast Computation of Radial Vibration in Switched Reluctance Motors', *IEEE Transactions on Industrial Electronics*, 2017, pp. 1-1.

[28] Zhong, R., Xu, Y., Cao, Y.P., Guo, X.Q., Hua, W., Xu, S., and Sun, W.F., 'Accurate Model of Switched Reluctance Motor Based on Indirect Measurement Method and Least Square Support Vector Machine', *IET Electric Power Applications*, vol. 10, no. 9, pp. 916-922, 2016.

[29] T. Zhangjun, P. Pillay, and A. M. Omekanda, "Vibration prediction in switched reluctance motors with transfer function identification from shaker and force hammer tests," *IEEE Transactions on Industry Applications*, vol. 39, pp. 978-985, 2003.

Xiaoqiang Guo (S'16) received the B.S. degree in measurement and control technology and instrumentation from Yangzhou University, Yangzhou, China, in 2012, and the M.S. degree in integrated circuit engineering from Southeast University, Nanjing, China, in 2015. He is currently pursuing the Ph.D. degree in microelectronics and solid-state electronics from Southeast University.

His research interests include design and control of switched reluctance motor with emphasis on analysis and reduction of vibration and noise of switched reluctance motor.

Rui Zhong received the B.S. degree in microelectronics and solid-state electronics from Xi'an Jiaotong University, Xi'an, China, in 1996, and the M.S. and Ph.D. degrees in microelectronics and solid-state electronics from Southeast University, Nanjing, China, in 2000 and 2003 respectively. He is currently an associate professor with the college of electronic science and engineering, Southeast University, Nanjing, China.

His research interests mainly include switched reluctance motor modeling and control, and analysis and optimization of motor drive system.

Mingshu Zhang received the B.S. degree in microelectronics from Northwestern Polytechnical University, Xi'an, China, in 2015, and he is currently working toward the M.S. degree in microelectronics and solid-state electronics from Southeast University, Nanjing, China.

His research interests mainly include integrated circuit design technology.

Desheng Ding received the B.S., M.S. and Ph.D. degrees in acoustic theory and application from Nanjing University, Nanjing, China, in 1986, 1989 and 1993 respectively. From 1993 to 1996, he was a postdoctoral researcher with the college of biological science and medical engineering, Southeast University, Nanjing, China. He is currently a professor with the college of electronic science and engineering, Southeast University, Nanjing, China from 1997.

His research interests mainly include sound surface wave theory and devices, ultrasonic transducer and nonlinear acoustics.

Weifeng Sun (SM'13) received the B.S., M.S. and Ph.D. degrees in electronic engineering from Southeast University, Nanjing, China, in 2000, 2003 and 2007 respectively. He was a visiting Scholar in the University of California, Irvine, US, in 2009. He is currently a professor with the college of electronic science and engineering, Southeast University, Nanjing, China from 2010.

His research interests mainly include new power device design, power IC, power device model, and power management system.